


RESEARCH

Open Access



Free breathing three-dimensional cardiac quantitative susceptibility mapping for differential cardiac chamber blood oxygenation – initial validation in patients with cardiovascular disease inclusive of direct comparison to invasive catheterization

Yan Wen^{1,2}, Jonathan W. Weinsaft³, Thanh D. Nguyen², Zhe Liu^{1,2}, Evelyn M. Horn³, Harsimran Singh³, Jonathan Kochav³, Sarah Eskreis-Winkler², Kofi Deh², Jiwon Kim³, Martin R. Prince², Yi Wang^{1,2} and Pascal Spincemaille^{2,4*} 

Abstract

Background: Differential blood oxygenation between left (LV) and right ventricles (RV; ΔSaO_2) is a key index of cardiac performance; LV dysfunction yields increased RV blood pool deoxygenation. Deoxyhemoglobin increases blood magnetic susceptibility, which can be measured using an emerging cardiovascular magnetic resonance (CMR) technique, Quantitative Susceptibility Mapping (QSM) – a concept previously demonstrated in healthy subjects using a breath-hold 2D imaging approach (2D_{BH}QSM). This study tested utility of a novel 3D free-breathing QSM approach (3D_{NAV}QSM) in normative controls, and validated 3D_{NAV}QSM for non-invasive ΔSaO_2 quantification in patients undergoing invasive cardiac catheterization (cath).

Methods: Initial control ($n = 10$) testing compared 2D_{BH}QSM (ECG-triggered 2D gradient echo acquired at end-expiration) and 3D_{NAV}QSM (ECG-triggered navigator gated gradient echo acquired in free breathing using a phase-ordered automatic window selection algorithm to partition data based on diaphragm position). Clinical testing was subsequently performed in patients being considered for cath, including 3D_{NAV}QSM comparison to cine-CMR quantified LV function ($n = 39$), and invasive-cath quantified ΔSaO_2 ($n = 15$). QSM was acquired using 3 T scanners; analysis was blinded to comparator tests (cine-CMR, cath).

(Continued on next page)

* Correspondence: pas2018@med.cornell.edu

²Department of Radiology, Weill Cornell Medicine, New York, NY, USA

⁴Weill Cornell Medical College, 515 East 71st Street, S101, New York, NY 10021, USA

Full list of author information is available at the end of the article



(Continued from previous page)

Results: 3D_{NAV}QSM generated interpretable QSM in all controls; 2D_{BH}QSM was successful in 6/10. Among controls in whom both pulse sequences were successful, RV/LV susceptibility difference (and ΔSaO_2) were not significantly different between 3D_{NAV}QSM and 2D_{BH}QSM (252 ± 39 ppb [$17.5 \pm 3.1\%$] vs. 211 ± 29 ppb [$14.7 \pm 2.0\%$]; $p = 0.39$). Acquisition times were 30% lower with 3D_{NAV}QSM (4.7 ± 0.9 vs. 6.7 ± 0.5 min, $p = 0.002$), paralleling a trend towards lower LV mis-registration on 3D_{NAV}QSM ($p = 0.14$). Among cardiac patients (63 ± 10 y, 56% CAD) 3D_{NAV}QSM was successful in 87% (34/39) and yielded higher ΔSaO_2 ($24.9 \pm 6.1\%$) than in controls ($p < 0.001$). QSM-calculated ΔSaO_2 was higher among patients with LV dysfunction as measured on cine-CMR based on left ventricular ejection fraction ($29.4 \pm 5.9\%$ vs. $20.9 \pm 5.7\%$, $p < 0.001$) or stroke volume ($27.9 \pm 7.5\%$ vs. $22.4 \pm 5.5\%$, $p = 0.013$). Cath measurements ($n = 15$) obtained within a mean interval of 4 ± 3 days from CMR demonstrated 3D_{NAV}QSM to yield high correlation ($r = 0.87$, $p < 0.001$), small bias (-0.1%), and good limits of agreement ($\pm 8.6\%$) with invasively measured ΔSaO_2 .

Conclusion: 3D_{NAV}QSM provides a novel means of assessing cardiac performance. Differential susceptibility between the LV and RV is increased in patients with cine-CMR evidence of LV systolic dysfunction; QSM-quantified ΔSaO_2 yields high correlation and good agreement with the reference of invasively-quantified ΔSaO_2 .

Keywords: Quantitative susceptibility mapping, Oxygenation, Cardiac magnetic resonance

Introduction

Differential blood oxygenation between the left and right heart (ΔSaO_2) is an established index of cardiac performance; left ventricular (LV) dysfunction results in stagnant blood flow – resulting in increased time for organ extraction of oxygen from blood and delivery of a greater fraction of deoxygenated blood to the right heart. Increased ΔSaO_2 has been shown to predict adverse prognosis in patients with heart failure with and without pulmonary hypertension [1–3] for whom it is commonly used to guide management [4, 5]. However, in current clinical practice, oxygen saturation is measured by invasive catheterization (cath). Non-invasive imaging methods to measure oxygenation in the heart are limited, prohibiting non-invasive quantification of cardiac blood pool oxygenation as part of routine clinical evaluation [6–13]. Given the fact that invasive catheterization entails procedural risks and can be challenging in critically ill patients [14–16], a non-invasive imaging method to accurately measure cardiac oxygenation would be of substantial clinical utility.

Quantitative susceptibility mapping (QSM) is an emerging cardiovascular magnetic resonance (CMR) technique that enables quantification of diamagnetic and paramagnetic materials [17–23]. Iron is a magnetically active element contained in hemoglobin that is central to oxygen transport - it is weakly diamagnetic when bound to oxygen, and paramagnetic when deoxygenated [24]. This change in magnetic susceptibility by deoxyheme [25, 26], provides a metric by which QSM can measure blood oxygen saturation. Prior work has validated QSM tissue characterization, including liver and brain iron content [22, 27–29]. Regarding blood oxygenation, a pilot study by our group showed cardiac QSM to be feasible in healthy subjects [30]. However, a 2D acquisition strategy was employed, which is suboptimal for imaging patients in

whom breath-holding is often compromised. To address this, a free-breathing 3D QSM approach was developed that uses diaphragmatic navigator gating to track respiratory position. This study compared 3D free-breathing QSM (3D_{NAV}QSM) to 2D breath held QSM (2D_{BH}QSM) in controls, as well as to the reference of ΔSaO_2 measured in patients undergoing invasive cardiac catheterization.

Methods

Study population

3D_{NAV}QSM was first compared to 2D_{BH}QSM among healthy subjects without clinically reported cardiovascular conditions or associated risk factors to test the relative performance in a cohort able to undergo prolonged imaging inclusive of both pulse sequences. Next, a second group of healthy subjects were scanned and rescanned to test the reproducibility of 3D_{NAV}QSM ΔSaO_2 measurement. The second group of healthy subjects was asked to get off and then get back on the table between the two scans. All healthy subjects were without self-reported cardiovascular disease or atherosclerosis risk factors.

After initial testing, 3D_{NAV}QSM was then performed among clinical patients who were being considered for or had undergone invasive catheterization to quantify blood oxygen saturation. Catheterization was performed by experienced physicians using standard techniques; intracardiac blood samples were obtained under baseline conditions (without supplemental O₂) and used to calculate ΔSaO_2 between the left and right heart. To test the effect of gadolinium in ΔSaO_2 measurement, QSM were obtained in 3 healthy subjects and in 4 patients both pre-contrast and ~ 30 min post-contrast administration.

This study was performed at Weill Cornell Medicine (WCM; New York, New York, USA). All participants (controls and patients) provided written informed consent

for research participation. This protocol was performed with the approval from the WCM Institutional Review Board.

Data acquisition

CMR was performed using commercial 3 T scanners (750/SIGNA, General Electric Healthcare, Waukesha Wisconsin, USA). $3D_{NAV}QSM$ and $2D_{BH}QSM$ imaging parameters were identical between healthy subjects and patients: $1^{st}TE/\Delta TE/\#TE/TR/BW = 2.3\text{ ms}/3.6\text{ ms}/5/20\text{ ms}/111.1\text{ kHz}$, acquisition matrix = 192×144 , slice thickness = 5 mm, views per heartbeat = 10, parallel imaging factor = 2. Full 3D flow compensation was implemented for both $2D_{BH}QSM$ and $3D_{NAV}QSM$ to minimize the phase generated by intra-chamber blood flow [26]. To shorten $3D_{NAV}QSM$ scan time, 75% partial Fourier acquisition was applied in the phase and slice encoding direction. Typical resolution is $1.5 \times 1.5 \times 5\text{ mm}^3$, 40 cm^2 FOV, and 20 slices per scan. Furthermore, $2D_{BH}QSM$ used electrocardiographic (ECG) gating and breath-holding, and $3D_{NAV}QSM$ used ECG and respiratory gating to ensure the acquisition of data at a consistent cardiac and respiratory phase. QSM was performed using non-contrast CMR in healthy subjects, and at the end of clinical exams in patients, which was approximately ~ 30 min post-gadolinium (Dotarem [gadoterate meglumine]; 0.2 mmol/kg) infusion. As stated above, in 3 healthy subjects and 4 patients, QSM was acquired both pre- and post-contrast.

$2D_{BH}QSM$ employed a conventional ECG-triggered multi-echo gradient echo sequence, for which data was acquired during end-expiration (~ 12 s per breath-hold). $3D_{NAV}QSM$ employed a tailored ECG-triggered navigator gated multi-echo gradient echo sequence, for which data was acquired during free breathing: a cross pair diaphragmatic navigator was used to track respiratory motion [31, 32]. A 2-bin phase-ordered automatic window selection (PAWS) gating algorithm (4 mm effective gating window) was used to tailor data acquisition according to diaphragm position in real-time [22]. In PAWS, each diaphragm position falls within a 2 mm bin for which k-space is acquired from alternating directions from bin to bin. The scan is complete when two adjacent bins have acquired all necessary k-space lines. Two navigator echoes were used in each heartbeat. The first navigator was acquired immediately before acquisition and used for PAWS gating. The second navigator was acquired immediately after data acquisition and used to provide additional motion suppression: if the difference between diaphragm positions detected by the two navigator echoes was > 4 mm for a given heartbeat, then the data acquired in that heartbeat were discarded and scheduled to be reacquired in a later heartbeat.

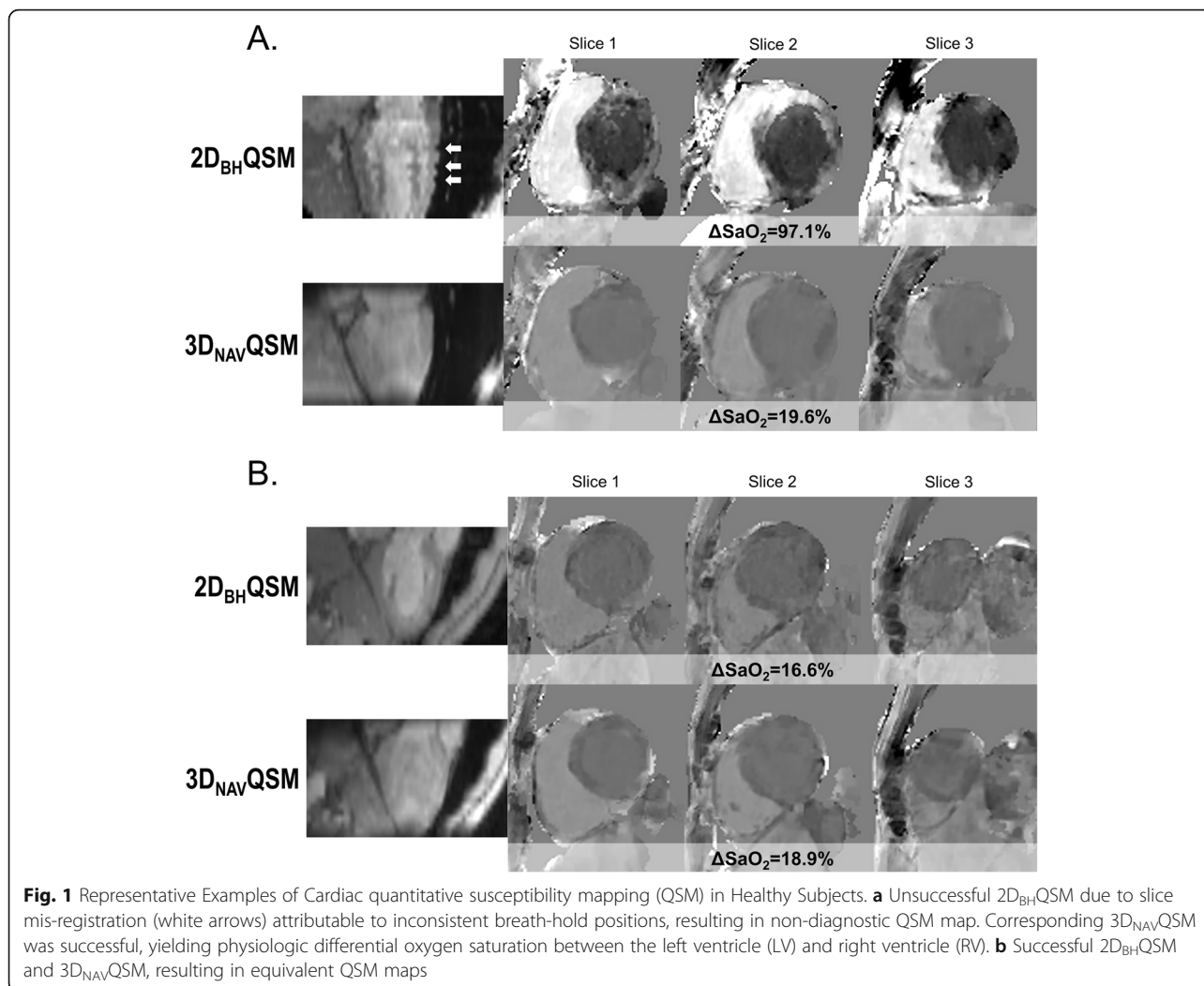
Ancillary imaging was performed to test QSM in relation to conventional cardiac functional/ remodeling indices. Cine-CMR was performed using a conventional balanced steady state free precession (bSSFP) pulse sequence with typical parameters: TE = 1.4 ms, TR = 3.8 ms, FA = 60° , bandwidth = 781 Hz/Px, resolution: $1.5 \times 1.5 \times 6\text{ mm}^3$, and SENSE acceleration R = 2, which was acquired in contiguous long and short axis images, the latter of which were segmented to quantify LV end-diastolic and end-systolic chamber volumes for calculation of LV and right ventricular (RV) ejection fraction (EF) as well as stroke volume.

QSM post processing

QSM maps were reconstructed by first obtaining a total field map (containing both the local and background field) with the contributions of fat chemical shift removed. This was done using both graph-cut based phase unwrapping [33] and IDEAL water/fat separation [34] with iterative chemical shift update [35]. Next, a susceptibility map was obtained using the preconditioned total field inversion method [36]. In this work, two regularization terms, similar to the regularization terms described in MEDI+0 [37], were added to the inversion to restrict the susceptibility variations within the RV and LV as follows:

$$y^* = \underset{y}{\operatorname{argmin}} \frac{1}{2} \|w(f-d \otimes Py)\|_2^2 + \lambda \|M_G \nabla Py\|_1 + \lambda_{RV} \|M_{RV} P(y - \bar{y}^{RV})\|_2^2 + \lambda_{LV} \|M_{LV} P(y - \bar{y}^{LV})\|_2^2 \quad (1)$$

The first two terms are the data fidelity term and structure consistency regularization term, respectively, where w is the signal to noise (SNR) weighting, f is the total field, d is the dipole kernel, \otimes is the convolution operator, P is the preconditioner, λ is the regularization parameter, M_G is a binary edge mask constructed by retaining the highest 70% of gradients of the T2* w image obtained by taking the square root of the sum of squares gradient recalled echo (GRE) images across echoes), and ∇ is the gradient operator [20], P is a binary mask that is 1 inside the region of interest (ROI) and a larger value, $P_{outside}$, outside of the ROI (see below). The final QSM map, χ , is then $\chi = Py^*$. The last two terms constrain the susceptibility variation within the RV and the LV blood pools, where λ_{RV} and λ_{LV} are the regularization parameters, M_{RV} and M_{LV} are the mask for RV and LV obtained through manual segmentation on the GRE images. \bar{y}^{RV} and \bar{y}^{LV} are the average susceptibility over the RV and LV blood pools, respectively. In this study, the values of $P_{outside} = 20$, $\lambda = 1/1000$, and $\lambda_{RV} = \lambda_{LV} = 1/20$ were empirically determined in an initial study in healthy subjects via visual



inspection of the corresponding QSM, and then fixed for subsequent subjects.

To account for potential field errors from water/fat separation, an iterative reweighted least squares fitting method, MERIT [38], was implemented to modify noise weighting of fat voxels (fat fraction > 30%) in each Gauss-Newton iteration to account for residual fat chemical shift not removed from the total field in the water/fat separation step. After iteration i in the Gauss-Newton solver, the noise weighting, w , in fat voxels for the next iteration $i + 1$ was recalculated as $w_{i+1}^* = \begin{cases} w_i & \frac{\rho_i}{2\sigma_i} \leq 1 \\ w_i / (\rho_i / 2\sigma_i) & \frac{\rho_i}{2\sigma_i} > 1 \end{cases}$, where $\rho_i = w_i |f - d * Py_i|$ is the voxel-by-voxel data term residual for the i th iteration, and σ_i is the standard deviation of ρ_i over all voxels.

The differential susceptibility between RV and LV blood pools ($\Delta\chi$) was converted to blood oxygenation difference (ΔSaO_2) using an established formula [30]:

$$\Delta SaO_2 = \frac{-\Delta\chi}{4H\chi_{deoxyheme}} \tag{2}$$

Where $\chi_{deoxyheme}$ is the molar susceptibility of deoxyheme such that $4\chi_{deoxyheme} = 151.054 \text{ ppb} \frac{\text{ml}}{\mu\text{mol}}$ is the molar susceptibility of a fully deoxygenated deoxyhemoglobin [39]. $H = 4Hct \frac{\rho_{RBC,Hb}}{M_{Hb}}$ is the heme concentration in blood (in $\mu\text{mol/ml}$), where Hct is the hematocrit, $\rho_{RBC,Hb} = 0.34 \frac{\text{g}}{\text{ml}}$ is the mass concentration of hemoglobin in a red blood cell, and $M_{Hb} = 64450 \times 10^{-6} \frac{\text{g}}{\mu\text{mol}}$ is the molar mass of deoxyhemoglobin. For controls, Hct was assumed to be 47% in men and 42% in women. These values were obtained by taking the average of the range in men and in women observed in a prior study [40]. For patients, Hct data was obtained from peripheral blood samples. Note that the current approach only measures the susceptibility difference between RV and LV blood pools (therefore only measures the oxygen saturation difference between the

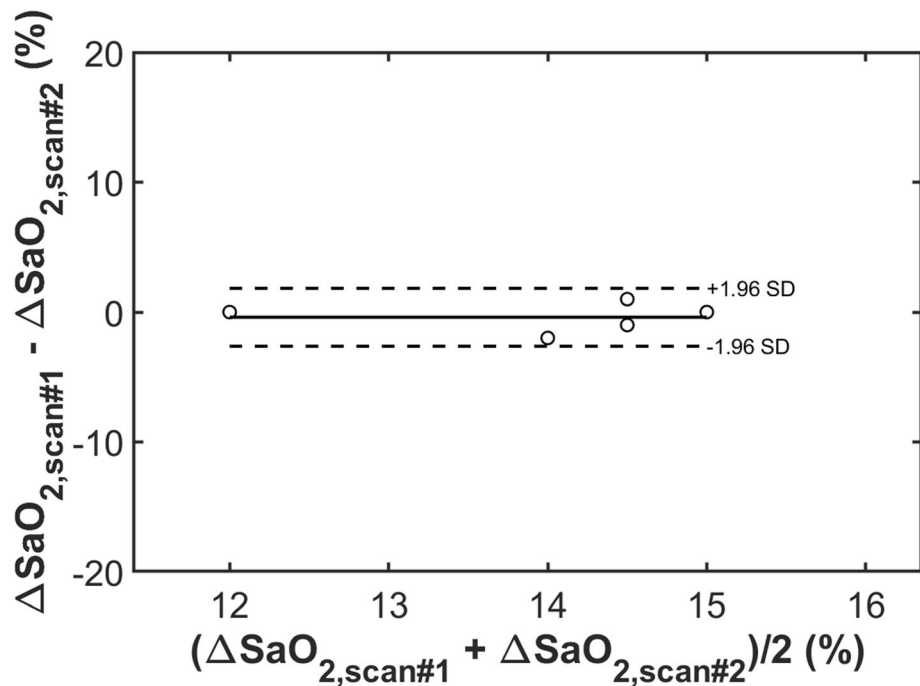


Fig. 2 ΔSaO_2 , QSM reproducibility experiment in normative controls $N=5$ healthy controls were scanned and rescanned to test the reproducibility of QSM based ΔSaO_2 measurement. The ΔSaO_2 measured by QSM between the two scans were very similar: small bias (-0.4%) and reasonable limits of agreement ($\pm 2.2\%$)

RV and LV blood pools), bypassing the need to reference the blood susceptibility to a susceptibility reference (typically chosen to be water), which may or may not replicate in-vivo conditions. Post-processing was performed using MATLAB (MathWorks, Natick, Massachusetts, USA).

QSM performance scores

Image quality (of GRE images) was assessed using two different approaches. Image quality for individual short axis slices (in-plane data) was scored semi-quantitatively based on visually assessed motion artifact/endocardial blurring (0 = severe, 1 = moderate, 2 = negligible). Scoring was performed by consensus of three experienced physicians (JWW, JK, JK). Through plane image quality was measured quantitatively based on the magnitude of slice misregistration (from both in-plane and through-plane motion), which was measured as the standard deviation of the second derivative along heart surface curves that were obtained from two perpendicular reformatted long-axis images that depict the heart-lung interface [30]: a higher standard deviation corresponded to lower through plane image quality (less smooth heart-lung interface).

Statistical methods

Continuous variables were compared between groups using Student's t-tests (expressed as mean \pm standard deviation). 2D and 3D image quality scores were compared

using a two-tailed Wilcoxon paired-sample signed rank test. Pearson correlation coefficients, Deming linear regression [41], and the Bland Altman plots were used to test the reproducibility in the two scans from the second group of healthy subjects, to test the associations between the QSM based ΔSaO_2 and the invasively quantified ΔSaO_2 , and to test the reproducibility in scans with and without contrast. Two-sided $p < 0.05$ was deemed indicative of statistical significance. Statistical analyses were performed using MATLAB and Prism 7 (GraphPad Software, La Jolla, California, USA).

Results

Normative controls

$3\text{D}_{\text{NAV}}\text{QSM}$ and $2\text{D}_{\text{BH}}\text{QSM}$ were acquired in a cohort of 10 healthy subjects (31 ± 4 y, 60% male). Whereas in-plane image quality (as visually assessed by three experienced physicians using a semi-quantitative score) was higher for $2\text{D}_{\text{BH}}\text{QSM}$ compared to $3\text{D}_{\text{NAV}}\text{QSM}$ (2.0 ± 0.0 vs. 1.1 ± 0.4 , $p < 0.001$), through plane image quality tended to be higher (lower slice misregistration) for $3\text{D}_{\text{NAV}}\text{QSM}$ compared to $2\text{D}_{\text{BH}}\text{QSM}$ ($1.0 \pm .2$ vs. $1.5 \pm .8$, $p = 0.14$).

$3\text{D}_{\text{NAV}}\text{QSM}$ successfully generated interpretable QSM in all 10 healthy subjects, whereas $2\text{D}_{\text{BH}}\text{QSM}$ was successful in only 6/10 (60%) of cases. Figure 1 provides a representative example of as an interpretable QSM dataset acquired by $3\text{D}_{\text{NAV}}\text{QSM}$ despite non-interpretable $2\text{D}_{\text{BH}}\text{QSM}$ (1A),

Table 1 Population characteristics

Age	63 ± 10yo
Gender (% male)	31% (12)
Known CAD	56% (22)
Pulmonary Hypertension	51% (20)
Atherosclerosis Risk Factors	
Tobacco Use (prior or current)	46% (18)
Hypertension	67% (26)
Hyperlipidemia	54% (21)
Diabetes mellitus	18% (7)
Medication Regimen	
ACE Inhibitors or ARB	51% (20)
Beta-Blockers	72% (28)
Aspirin	74% (29)
Statin	69% (27)
Diuretic	46% (18)
Cardiac Structure/Function	
LVEF (%)	49 ± 14%
LV Dysfunction (EF < 50%)	49% (19)
LV End-Diastolic Volume	186 ± 57 ml
LV End-Systolic Volume	106 ± 56 ml
RV EF (%)	51 ± 11%
RV Dysfunction (EF < 50%)	31% (12)
RV End-Diastolic Volume	169 ± 62 ml
RV End-Systolic Volume	96 ± 52 ml

Data reported as % (n) for categorical variables, mean standard deviation for continuous variables

ACE angiotensin converting enzyme, ARB angiotensin receptor blocker, CAD coronary artery disease, EF ejection fraction, LV left ventricle, RV right ventricular

as well an interpretable QSM dataset concordantly acquired by 2D_{BH}QSM and 3D_{NAV}QSM (**1B**).

In all cases for which 2D_{BH}QSM was uninterpretable, failure was due to slice misregistration between sequential LV short axis datasets. Consistent with this, quantitative slice misregistration was over 2-fold higher in cases for which 2D_{BH}QSM failed ($n = 4$) compared to cases ($n = 6$) in which 2D_{BH}QSM yielded diagnostic results (2.3 ± 0.4 vs. 1.0 ± 0.2 , $p < 0.001$). There was no significant difference in slice misregistration between 3D_{NAV}QSM and 2D_{BH}QSM in exams for which both sequences were successful (1.0 ± 0.1 vs. 1.0 ± 0.2 , $p = 1.0$).

Regarding data acquisition time, results demonstrated 3D_{NAV}QSM to yield a 30% reduction compared to 2D_{BH}QSM (4.7 ± 0.9 vs. 6.7 ± 0.5 min, $p = 0.002$) attributable to the interval time between each breath-hold. Navigator efficiency for 3D_{NAV}QSM was $54 \pm 12\%$. Reduced scan time yielded by 3D_{NAV}QSM remained significant even among controls in whom both pulse sequences produced diagnostic results and acquisitions were reduced by an

average of 37% (4.3 ± 1.4 vs. 6.8 ± 0.4 min, $p = 0.002$), with navigator efficiency for 3D_{NAV}QSM $56 \pm 16\%$.

Regarding QSM results, mean RV/LV susceptibility difference was not significantly different between 3D_{NAV}QSM and 2D_{BH}QSM acquired in controls in whom the latter pulse sequence was successful (252 ± 39 ppb vs. 211 ± 29 ppb, $p = 0.39$), corresponding to ΔSaO_2 of $17.5 \pm 3.1\%$ and $14.7 \pm 2.0\%$, respectively. Of note, the RV/LV susceptibility difference (and ΔSaO_2) calculated using 3D_{NAV}QSM was not significantly different when compared between controls with and without diagnostic results yielded by 2D_{BH}QSM (252 ± 39 ppb vs. 250 ± 33 ppb, $p = 0.87$ [$17.5 \pm 3.1\%$ vs. $17.3 \pm 2.4\%$]).

Reproducibility of 3D_{NAV}QSM (as tested in 5 healthy subjects) was high, as evidenced by small mean differences (-0.4%) and reasonable limits of agreement ($\pm 2.2\%$) between data acquired during two separate scans (Fig. 2).

Clinical patients

3D_{NAV}QSM was acquired in 39 patients whose population characteristics are shown in Table 1. In this group, QSM data was successfully obtained in 87% (34/39) of cases. In 5 cases, 3D_{NAV}QSM yielded non-diagnostic results (non-physiological equivalence between LV and RV blood oxygenation) – all of which had substantial motion artifact. In the remainder of patients ($n = 34$), RV/LV susceptibility difference calculated using 3D_{NAV}QSM was substantial (298 ± 72 ppb), corresponding to a ΔSaO_2 of $24.9 \pm 6.1\%$ ($p < 0.001$ vs. controls). Image acquisition time in the overall clinical cohort was 6.9 ± 2.8 min; increased acquisition time tended to be longer among patients compared to controls (4.7 ± 0.9 min; $p = 0.04$) due to greater respiratory variability and lower navigator efficiency in patients ($36 \pm 12\%$ vs. $54 \pm 12\%$).

Among the overall clinical cohort in whom QSM was successful ($n = 34$), results varied in relation to LV systolic dysfunction as quantified using cine-CMR. As shown in Fig. 3a, a greater ΔSaO_2 on QSM was observed among patients with LV dysfunction (EF < 50%) as quantified by cine-CMR ($29.4 \pm 5.9\%$ vs. $20.9 \pm 5.7\%$, $p < 0.001$). Similarly, patients in the bottom median of cine-CMR quantified LV stroke volume had greater ΔSaO_2 on QSM ($27.9 \pm 7.5\%$ vs. $22.4 \pm 5.5\%$, $p = 0.013$).

In a subgroup of 15 patients who had successful QSM, invasive cardiac catheterization (cath) was available as a reference standard for heart chamber oxygenation: all patients underwent catheterization for evaluation of known/suspected heart failure – 47% had LV systolic dysfunction and 53% had primary pulmonary hypertension. Mean interval between tests (cath, CMR) was 4 ± 3 days (range 0–12 days). Figure 3b provides representative patient examples, including close agreement with invasively quantified ΔSaO_2 and increased magnitude of difference in

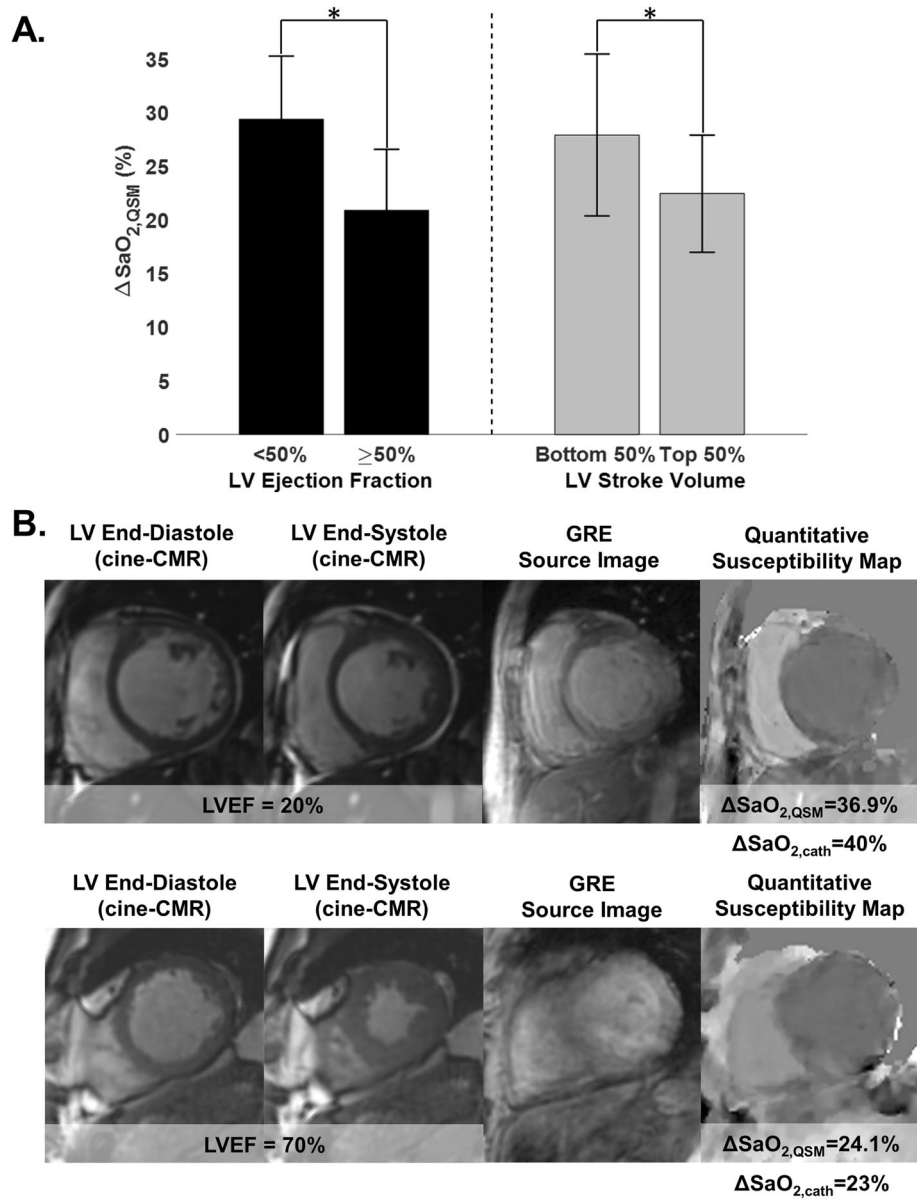


Fig. 3 Cardiac QSM in Cardiac Patients. **a** QSM ΔSaO_2 among patients grouped based on presence or absence of LV systolic dysfunction based on cine-CMR quantified ejection fraction (left) and stroke volume (right) (data shown as mean \pm standard deviation). Note greater ΔSaO_2 among patients with LV systolic dysfunction. **b** Two representative examples of QSM maps in cardiac patients. In the top patient, who had severely reduced LV function (EF = 20%), QSM measured a marked increase in ΔSaO_2 (36.9%), which agreed well with invasive catheterization (40%). In the bottom patient, who had normal LV function (EF = 70%), QSM measured ΔSaO_2 (24.1%) was within normal limits and was similar to invasive data (23%)

context of LV dysfunction. As shown in Fig. 4a, QSM yielded good correlation with invasively quantified ΔSaO_2 ($r = 0.87$, $p < 0.001$); corresponding to small bias (-0.1%) and reasonable limits of agreement ($\pm 8.6\%$) between the two tests (Fig. 4b). Table 2 provides a breakdown of QSM results on a per-patient basis, together with invasive cath data and corresponding indices of LV function. Consistent with results in the overall clinical cohort, patients who underwent cath demonstrated LV systolic dysfunction

(EF < 50%) to be associated with greater ΔSaO_2 on both invasive testing ($32.9 \pm 3.7\%$ vs. $21.2 \pm 6.9\%$, $p = 0.002$) and non-invasive QSM ($33.9 \pm 5.6\%$ vs. $21.2 \pm 5.8\%$, $p < 0.001$).

Cardiac QSM before and after contrast administration

3D_{NAV}QSM was obtained successfully in all 7 subjects who were scanned both before and after contrast administration. As shown in Fig. 5, the ΔSaO_2 measured from pre- and post-contrast QSM matched very well (slope =

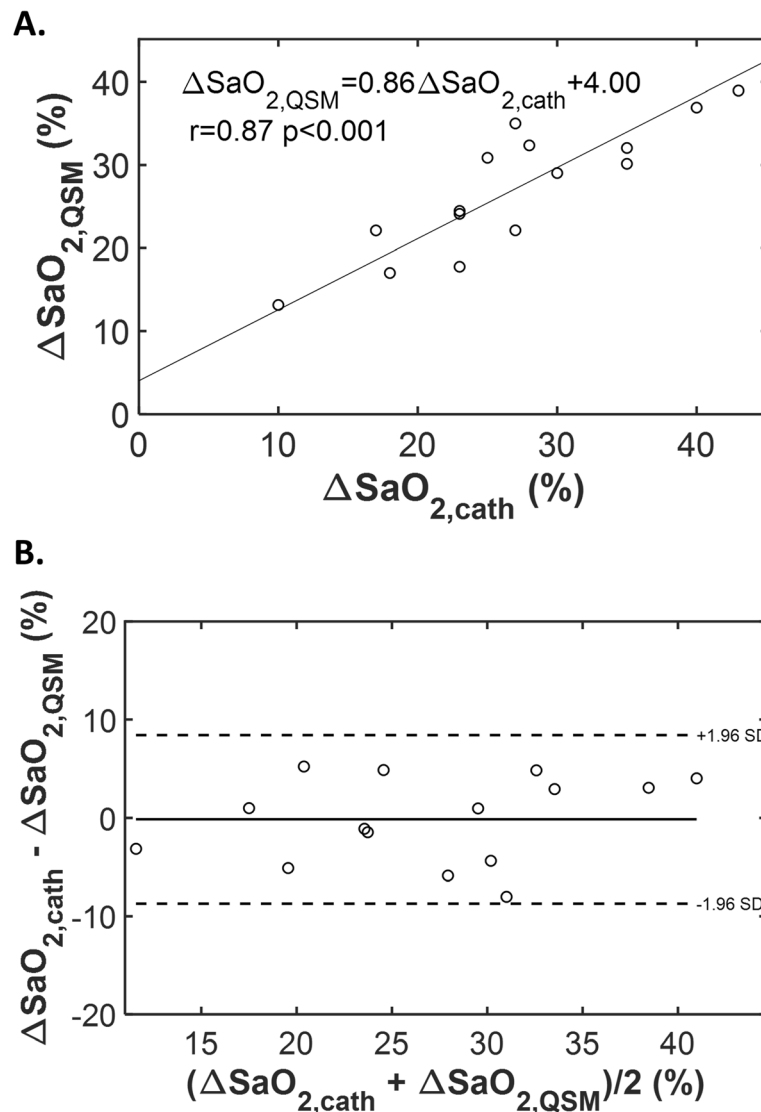


Fig. 4 Cardiac QSM in Relation to Invasive Catheterization. **a** Scatter plot examining QSM derived ΔSaO_2 in relation to invasive catheterization derived ΔSaO_2 . A good correlation ($r = 0.87$, $p < 0.001$) and linear relationship between the two approaches is observed. **b** Bland Altman plot. Note small bias between the two tests (-1.1%) and moderate limits of agreement ($\pm 8.6\%$)

1.04, $r = 0.97$, $p < 0.001$), with a small bias (-0.7%), small limits of agreement ($\pm 1.9\%$), and a small mean absolute difference (0.9%).

Discussion

This is the first study to test the free breathing 3D cardiac QSM for non-invasive measurement of blood oxygenation, inclusive of validation data provided by cine-CMR quantified cardiac remodeling and invasively quantified oxygen saturation in cardiac patients. Key findings are as follows: first, among a normative test cohort, $3\text{D}_{\text{NAV}}\text{QSM}$ had a greater success for interpretable results than did $2\text{D}_{\text{BH}}\text{QSM}$ (100% vs. 60%) and did so within shorter scan time. Second, $3\text{D}_{\text{NAV}}\text{QSM}$ performed robustly in a

subsequent cohort of 39 patients with established cardiovascular disease, among whom results demonstrated differential LV/RV susceptibility in 87% (34/39) of cases: magnitude of ΔSaO_2 differed in relation to LV systolic dysfunction as quantified on cine-CMR, as evidenced by greater ΔSaO_2 on QSM among patients with impaired LVEF ($< 50\%$) compared to those with preserved LVEF, and similar results when QSM results were compared in relation to decreased LV function as stratified based on stroke volume. Third, among a subgroup of patients undergoing invasive catheterization, $3\text{D}_{\text{NAV}}\text{QSM}$ yielded good correlation with invasively quantified ΔSaO_2 , corresponding to reasonably small bias and limits of agreement (-0.1 and $\pm 8.6\%$, respectively) between approaches.

Table 2 QSM in relation to Invasive Catheterization ΔSaO_2 and Cine-CMR Cardiac Function

Patient	cath ΔSaO_2 (%)	QSM ΔSaO_2 (%)	LV Ejection Fraction (%)	LV Stroke Volume (ml)	LV Dysfunction (1 = EF < 50%)	Pulmonary Hypertension (1 = present)
1	25	31	66	96	0	1
2	17	22	70	60	0	0
3	23	24	71	140	0	0
4	10	13	70	90	0	0
5	35	32	47	71	1	1
6	30	29	28	77	1	0
7	40	37	20	48	1	0
8	43	39	20	60	1	1
9	27	35	16	66	1	1
10	28	32	40	48	1	1
11	27	22	66	28	0	1
12	35	30	33	47	1	1
13	23	18	65	94	0	0
14	23	24	54	126	0	0
15	18	17	69	93	0	1

While our data validate cardiac QSM for differential chamber oxygenation, it is important to recognize that prior research has applied different CMR approaches for this purpose. Most previous approaches are based on measurement of blood CMR relaxation times (T2, T2*, and T1) [6–10, 12, 13, 42]. However, conventional methods based on longitudinal (T1) or transverse (T2) relaxation properties can be challenging to apply clinically. For example, the dependence of spin echo T2 on oxygenation is well understood, but in practice requires measuring several model parameters in addition to oxygenation, thereby potentially limiting accuracy or complicating clinical implementation. Recently, an oxygen saturation measurement based on acquiring multiple T2 maps using a 2D T2 prepared bSSFP sequence designed to overcome these limitations was shown to provide good agreement with invasive catheterization based measurement in an animal study. A comparison between this promising approach and our proposed QSM approach is warranted in a future study [11]. An alternative approach consists of quantifying the magnetic susceptibility of blood. The physical model relating blood susceptibility to oxygen saturation is simpler than that for T2 as it is linear with the slope a known physical constant. The magnetic susceptibility of venous blood can be computed from the CMR image phase by geometric modeling [43–47]. Mapping of magnetic susceptibility throughout the 3D field of view, as is done in QSM, enables measurement of oxygen saturation of any vascular structure (including the heart) by simple ROI analysis [25, 26, 48]. Our current data extends on prior work by our group that has shown QSM to provide an index of

hemorrhage [26, 28], as well as an index of metabolism and oxygen utilization in the brain [49, 50].

Our QSM results regarding differential LV and RV blood oxygen saturation are consistent with values reported in prior literature as well as expected differences between subjects with and without cardiovascular disease. Regarding control data, ΔSaO_2 measured from 3D_{NAV}QSM ($17.5 \pm 3.1\%$) was in agreement with a prior study that reported ΔSaO_2 in healthy subjects undergoing invasive cardiac catheterization [51], in which a mean difference of 18.8% was reported (arterial: 97.3%, venous: 78.5%). ΔSaO_2 as measured in controls were also lower than that in patients with cardiovascular disease ($17.5 \pm 3.1\%$ vs. $24.9 \pm 6.1\%$, $p < 0.001$), consistent with expected physiological differences between the two groups. Among our subgroup of patients with cath validation ($n = 15$), QSM derived ΔSaO_2 demonstrated a linear relationship with invasive measurements, and bias between the two oxygenation measurement approaches was small. While our data cannot be interpreted in context of an exact partition value with which to guide clinical decision making, it should be noted that an array of studies have demonstrated prognosis to vary in relation to magnitude of differential oxygen saturations between the left and right heart [1–5]. In this context, our findings suggest promise for development of QSM derived ΔSaO_2 as a non-invasive risk stratification tool, such that clinically stable patients with normal values would be screened out as low risk, whereas those with elevated QSM derived ΔSaO_2 are referred for confirmatory invasive testing.

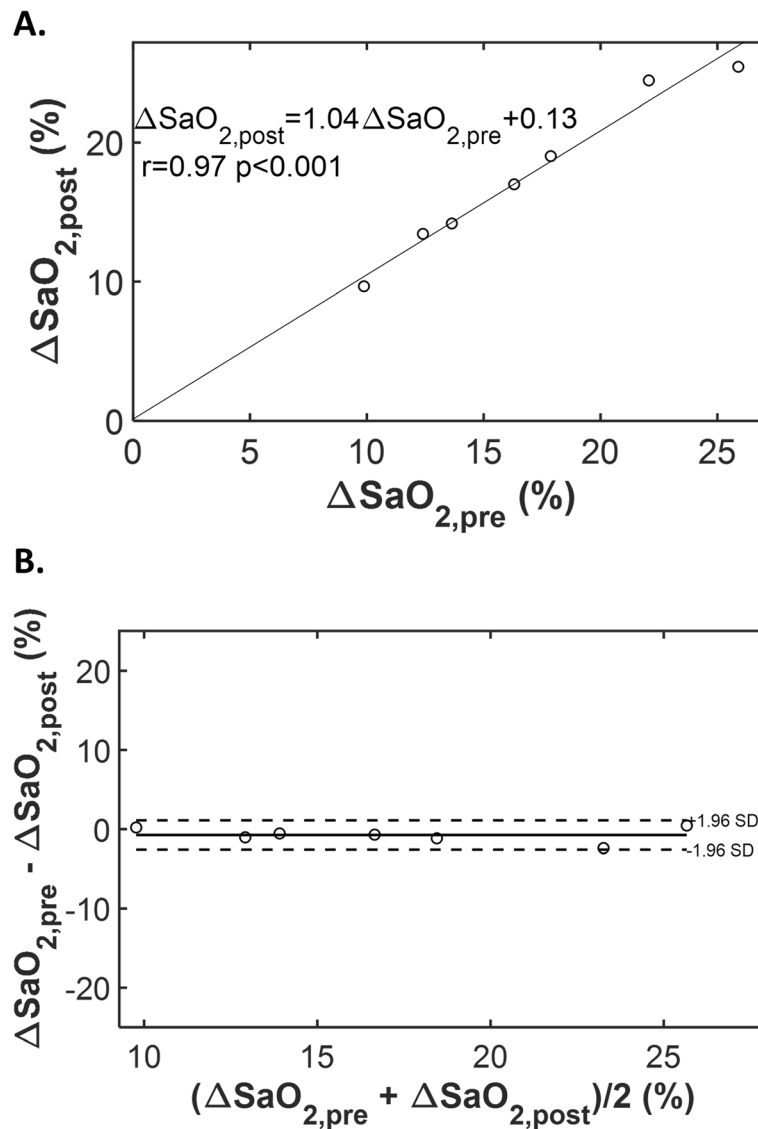


Fig. 5 QSM based ΔSaO_2 measured pre- and post-contrast administration. **a** Scatter plot examining QSM derived ΔSaO_2 pre- and post-contrast administration. A good correlation and linear relationship between the two measurements is observed. **b** Bland Altman plot showing small bias (-0.7%) and small limits of agreement ($\pm 1.9\%$)

Note that, in this work, QSM was performed during non-contrast imaging in healthy subjects, and at the end of contrast-enhanced exams (~ 30 min post gadolinium infusion) in patients. Whereas gadolinium changes blood susceptibility, prior data has shown gadolinium to be near completely cleared from myocardium, and to be well mixed in the intravascular space at our imaging time point [52, 53]. Accordingly, QSM calculations were based on the premise that contrast blood pool concentration was constant across cardiac chambers, such that gadolinium contributions to susceptibility in the LV and RV cancel out when computing differential oxygenation. Indeed, our data demonstrate that cardiac QSM derived ΔSaO_2 measurements agree well between pre- and post-contrast.

One key technical innovation in our current study concerns use of navigator technology for free breathing 3D QSM. The conventional cardiac 2D_{BH} QSM approach generates data by imaging LV (short axis) slices individually via sequential breath-holds in order to reconstruct a 3D field map. When one or more of these breath-holds is acquired at a different respiratory position than the others, the resulting field map will not be a true 3D volume, and the QSM map will contain artifacts as the reconstruction model assumes a continuous 3D dataset as input. The susceptibility inversion problem is inherently 3D, given that susceptibility changes within one region of a given structure (e.g. RV blood pool) affects the field in the surrounding areas in all three (x, y,

z) spatial directions: this is because the field is a 3D convolution of the underlying 3D susceptibility distribution with the dipole kernel. The 3D_{NAV}QSM approach has no inherent mis-registration limitation, and the success of 3D_{NAV}QSM acquisition depends on navigator accuracy in motion tracking. These aspects of QSM reconstruction may explain our seemingly discordant finding regarding GRE image quality and diagnostic performance of the two QSM pulse sequences tested in our study: even though GRE images from the 2D_{BH}QSM sequence were assigned higher image scores than images from the 3D_{NAV}QSM sequence, 2D_{BH}QSM failed to generate interpretable QSM more often than did 3D_{NAV}QSM and this failure was primarily attributable to slice mis-registration.

There are several limitations of our study. First, scan time of 3D_{NAV}QSM sequence is long (~4–7 min) compared to other routine clinical sequences. One potential approach to shorten scan time is to increase parallel acceleration factor, use compressed sensing [54, 55], and/or apply data acquisition strategies such as echo planar readout [56] or echo sharing methods [57]. Non-Cartesian acquisitions that allow for self-gating [58] and multi-phase reconstruction [59] are also alternatives to shorten cardiac QSM. A second limitation to the current 3D_{NAV}QSM approach is that the respiratory motion is tracked by a diaphragmatic navigator, which is known to occasionally fail [60]. More advanced navigator techniques such as a fat navigator can be used to improve success rates [31, 32, 61–63]. A third issue to consider is that the QSM validation in this study was derived from cardiac remodeling indices in 39 cardiac patients of whom 15 had invasive catheterization for evaluation of known or suspected heart failure; further validation in a larger clinical cohort including patients undergoing catheterization for different indications is warranted. Finally, whereas the interval between QSM and invasive catheterization was relatively short (mean 4 ± 3 days, median 2 days [IQR 1–5 days]), cardiac chamber oxygenation could have varied during this time, thus resulting in discordance between tests. Future research with simultaneous invasive and CMR oxygenation measurements in animal models could be of utility for further validation of QSM, as well as comparisons with alternative pulse sequences for oxygenation quantification (i.e. T2). Nevertheless, our current findings that 3D navigator QSM was feasible among a clinical cohort in whom it generally agreed with differential oxygenation saturation as measured invasively is of substantial importance with respect to translational application of this technique, and provides initial proof of concept with respect to clinical implementation.

Heart rate could have impacted our QSM results. This has been shown to be the case for oxygenation methods

such as BOLD, which relies on the magnitude of the CMR signal. On the other hand, QSM, which relies on the phase of the CMR signal, is expected to be relatively insensitive to heart rate because the contributions to the phase (field) induced by the difference in LV and RV magnetic susceptibility (oxygenation) are not affected by heart rate. Further research is warranted to specifically assess physiologic factors impacting QSM, as well as to validate this pulse sequence in a larger clinical cohort including patients undergoing catheterization for different indications.

In conclusion, we provide validation of free breathing 3D cardiac QSM as an index of cine-CMR evidenced LV dysfunction and differential LV/RV oxygen saturation as measured by invasive catheterization. Future research is necessary to test accelerated free-breathing QSM strategies, refine cardiac QSM for myocardial tissue characterization, and validate QSM-derived blood oxygenation for non-invasive stratification of heart failure symptoms and prognostic outcomes.

Abbreviations

2D_{BH}QSM: 2D Breath-hold QSM approach; 3D_{NAV}QSM: 3D free-breathing QSM approach; bSSFP: balanced steady state free precession; cath: Catheterization; CMR: Cardiovascular magnetic resonance; ECG: Electrocardiogram; EF: Ejection fraction; GRE: Gradient recalled echo; Hct: Hematocrit; IDEAL: Iterative decomposition of water and fat with echo asymmetry and least squares estimation; LV: Left ventricle/left ventricular; MEDI: Morphology enabled dipole inversion; MERIT: An iterative reweighted least squares fitting method; O₂: Oxygen; PAWS: Phase-ordered automatic window selection; QSM: Quantitative susceptibility mapping; RHC: Right heart catheterization; ROI: Region of interest; RV: Right ventricle/right ventricular; SNR: Signal-to-noise ratio; TE: Echo time; TR: Repetition time; ΔSaO₂: Differential blood oxygenation between the left and right heart

Acknowledgements

Not applicable.

Authors' contributions

Author contributions are as follows: conception and study design (YW1, JWW, TDN, YW2, PS), development of algorithms and analysis software, data collection and protocol design (YW1, JWW, TDN, ZL, EMH, HS, JK, SEW, KD, JW, MRP, YW2, PS), data analysis (YW1, TDN, JWW, PS), interpretation of data and results (YW1, TDN, JWW, PS), and writing of manuscript (YW1, TDN, JWW, YW2, PS). All authors read and approved the final manuscript.

Funding

National Institutes of Health, grant #s R01HL128278–01 (JWW, JK), NIH 1 K23 HL140092–01 (JK), R01HL128278 (YW2), R01NS072370 (YW2), R01NS090464 (YW2), R01NS095562 (YW2), R01CA181566 (PS), Society for Cardiovascular Magnetic Resonance Seed Grant (YW1), Weill Cornell Medicine/Citigroup Biomedical Imaging Center Radiology Investigation Grant (PS).

Availability of data and materials

The datasets generated and/or analyzed during the current study are available from the corresponding author on reasonable request.

Ethics approval and consent to participate

Data usage for this study was approved by the Institutional Review Boards at New York Presbyterian Hospital/Weill Cornell Medicine; all subjects provided written informed consent for research participation.

Consent for publication

Not applicable.

Competing interests

YW2 and PS are inventors on a patent describing QSM and hold equity in Medimagemetric LLC. The remaining authors declare that they have no competing interests.

Author details

¹Meinig School of Biomedical Engineering, Cornell University, Ithaca, NY, USA. ²Department of Radiology, Weill Cornell Medicine, New York, NY, USA. ³Department of Medicine, Weill Cornell Medicine, New York, NY, USA. ⁴Weill Cornell Medical College, 515 East 71st Street, S101, New York, NY 10021, USA.

Received: 2 January 2019 Accepted: 4 October 2019

Published online: 18 November 2019

References

- Gallet R, Lellouche N, Mitchell-Heggs L, Bouhemad B, Bensaid A, Dubois-Randé J-L, Gueret P, Lim P. Prognosis value of central venous oxygen saturation in acute decompensated heart failure. *Archives of Cardiovascular Diseases*. 2012;105(1):5–12.
- Swiston JR, Johnson SR, Granton JT. Factors that prognosticate mortality in idiopathic pulmonary arterial hypertension: a systematic review of the literature. *Respir Med*. 2010;104(11):1588–607.
- Sandoval J, Bauerle O, Palomar A, Gomez A, Martinez-Guerra ML, Beltran M, Guerrero ML. Survival in primary pulmonary hypertension. Validation of a prognostic equation. *Circulation*. 1994;89(4):1733–44.
- Mullens W, Abrahams Z, Skouri HN, Taylor DO, Starling RC, Francis GS, Young JB, Tang WH. Prognostic evaluation of ambulatory patients with advanced heart failure. *Am J Cardiol*. 2008;101(9):1297–302.
- Patel CB, DeVore AD, Felker GM, Wojdyla DM, Hernandez AF, Milano CA, O'Connor CM, Rogers JG. Characteristics and outcomes of patients with heart failure and discordant findings by right-sided heart catheterization and cardiopulmonary exercise testing. *Am J Cardiol*. 2014;114(7):1059–64.
- Li D, Wang Y, Waight DJ. Blood oxygen saturation assessment in vivo using T2* estimation. *Magn Reson Med*. 1998;39(5):685–90.
- Silvennoinen MJ, Kettunen MI, Kauppinen RA. Effects of hematocrit and oxygen saturation level on blood spin-lattice relaxation. *Magn Reson Med*. 2003;49(3):568–71.
- Wright GA, Hu BS, Macovski A. Estimating oxygen saturation of blood in vivo with MR imaging at 1.5 T. *J Magn Reson Imaging*. 1991;1(3):275–83.
- Thulborn KR, Waterton JC, Matthews PM, Radda GK. Oxygenation dependence of the transverse relaxation time of water protons in whole blood at high field. *Biochim Biophys Acta Gen Subj*. 1982;714(2):265–70.
- Lu H, Ge Y. Quantitative evaluation of oxygenation in venous vessels using T2-relaxation-under-spin-tagging MRI. *Magn Reson Med*. 2008;60(2):357–63.
- Varghese J, Potter LC, LaFountain R, Pan X, Raman SV, Ahmad R, Simonetti OP. CMR-based blood oximetry via multi-parametric estimation using multiple T2 measurements. *J Cardiovasc Magn Reson*. 2017;19(1):88.
- Ogawa S, Menon RS, Tank DW, Kim SG, Merkle H, Ellermann JM, Ugurbil K. Functional brain mapping by blood oxygenation level-dependent contrast magnetic resonance imaging. A comparison of signal characteristics with a biophysical model. *Biophys J*. 1993;64(3):803–12.
- Bolar DS, Rosen BR, Sorensen AG, Adalsteinsson E. Quantitative imaging of extraction of oxygen and tissue consumption (QUIXOTIC) using venular-targeted velocity-selective spin labeling. *Magn Reson Med*. 2011;66(6):1550–62.
- Judge O, Ji F, Fleming N, Liu H. Current use of the pulmonary artery catheter in cardiac surgery: a survey study. *J Cardiothorac Vasc Anesth*. 2015;29(1):69–75.
- Browman EY, Gabriel RA, Dutton RP, Urman RD. Pulmonary artery catheter use during cardiac surgery in the United States, 2010 to 2014. *J Cardiothorac Vasc Anesth*. 2016;30(3):579–84.
- Jesurum J. Svo2 Monitoring. *Crit Care Nurse*. 2004;24(4):73–6.
- de Rochefort L, Liu T, Kressler B, Liu J, Spincemaille P, Lebon V, Wu J, Wang Y. Quantitative susceptibility map reconstruction from MR phase data using bayesian regularization: validation and application to brain imaging. *Magn Reson Med*. 2010;63(1):194–206.
- Haacke EM, Liu S, Buch S, Zheng W, Wu D, Ye Y. Quantitative susceptibility mapping: current status and future directions. *Magn Reson Imaging*. 2015; 33(1):1–25.
- Liu C, Li W, Tong KA, Yeom KW, Kuzminski S. Susceptibility-weighted imaging and quantitative susceptibility mapping in the brain. *J Magn Reson Imaging*. 2015;42(1):23–41.
- Wang Y, Liu T. Quantitative susceptibility mapping (QSM): decoding MRI data for a tissue magnetic biomarker. *Magn Reson Med*. 2015;73(1):82–101.
- Schweser F, Deistung A, Reichenbach JR. Foundations of MRI phase imaging and processing for quantitative susceptibility mapping (QSM). *Z Med Phys*. 2016;26(1):6–34.
- Wang Y, Spincemaille P, Liu Z, Dimov A, Deh K, Li J, Zhang Y, Yao Y, Gillen KM, Wilman AH, Gupta A, Tsiouris AJ, Kovanlikaya I, Chiang GC-Y, Weinsaft JW, Tanenbaum L, Chen W, Zhu W, Chang S, Lou M, Kopell BH, Kaplitt MG, Devos D, Hirai T, Huang X, Korogi Y, Shtilbans A, Jahng G-H, Pelletier D, Gauthier SA, Pitt D, Bush AI, Brittenham GM, Prince MR. Clinical quantitative susceptibility mapping (QSM): Biometal imaging and its emerging roles in patient care. *Journal of Magnetic Resonance Imaging*. 2017;46(4):951–71.
- Zhou D, Cho J, Zhang J, Spincemaille P, Wang Y. Susceptibility underestimation in a high-susceptibility phantom: dependence on imaging resolution, magnitude contrast, and other parameters. *Magn Reson Med*. 2017;78(3):1080–6.
- Pauling L, Coryell CD. The magnetic properties and structure of hemoglobin, Oxyhemoglobin and Carbonmonoxyhemoglobin. *Proc Natl Acad Sci U S A*. 1936;22(4):210–6.
- Fan AP, Bilgic B, Gagnon L, Witzel T, Bhat H, Rosen BR, Adalsteinsson E. Quantitative oxygenation venography from MRI phase. *Magn Reson Med*. 2014;72(1):149–59.
- Xu B, Liu T, Spincemaille P, Prince M, Wang Y. Flow compensated quantitative susceptibility mapping for venous oxygenation imaging. *Magn Reson Med*. 2014;72(2):438–45.
- Dimov AV, Liu Z, Spincemaille P, Prince MR, Du J, Wang Y. Bone quantitative susceptibility mapping using a chemical species-specific R2* signal model with ultrashort and conventional echo data. *Magn Reson Med*. 2018;79(1):121–8.
- Chen W, Zhu W, Kovanlikaya I, Kovanlikaya A, Liu T, Wang S, Salustri C, Wang Y. Intracranial calcifications and hemorrhages: characterization with quantitative susceptibility mapping. *Radiology*. 2014;270(2):496–505.
- Zhang J, Zhou D, Nguyen TD, Spincemaille P, Gupta A, Wang Y. Cerebral metabolic rate of oxygen (CMRO2) mapping with hyperventilation challenge using quantitative susceptibility mapping (QSM). *Magnetic Resonance in Medicine*. 2016. <https://doi.org/10.1002/mrm.26253>.
- Wen Y, Nguyen TD, Liu Z, Spincemaille P, Zhou D, Dimov A, Kee Y, Deh K, Kim J, Weinsaft JW, Wang Y. Cardiac quantitative susceptibility mapping (QSM) for heart chamber oxygenation. *Magn Reson Med*. 2018;79(3):1545–52.
- Nguyen TD, Spincemaille P, Weinsaft JW, Ho BY, Cham MD, Prince MR, Wang Y. A fast navigator-gated 3D sequence for delayed enhancement MRI of the myocardium: comparison with breathhold 2D imaging. *J Magn Reson Imaging*. 2008;27(4):802–8.
- Nguyen TD, Spincemaille P, Cham MD, Weinsaft JW, Prince MR, Wang Y. Free-breathing 3-dimensional steady-state free precession coronary magnetic resonance angiography: comparison of four navigator gating techniques. *Magn Reson Imaging*. 2009;27(6):807–14.
- Dong J, Liu T, Chen F, Zhou D, Dimov A, Raj A, Cheng Q, Spincemaille P, Wang Y. Simultaneous phase unwrapping and removal of chemical shift (SPURS) using graph cuts: application in quantitative susceptibility mapping. *IEEE Trans Med Imaging*. 2015;34(2):531–40.
- Reeder SB, Pineda AR, Wen Z, Shimakawa A, Yu H, Brittain JH, Gold GE, Beaulieu CH, Pelc NJ. Iterative decomposition of water and fat with echo asymmetry and least-squares estimation (IDEAL): application with fast spin-echo imaging. *Magn Reson Med*. 2005;54(3):636–44.
- Dimov AV, Liu T, Spincemaille P, Ecanow JS, Tan H, Edelman RR, Wang Y. Joint estimation of chemical shift and quantitative susceptibility mapping (chemical QSM). *Magn Reson Med*. 2015;73(6):2100–10.
- Liu Z, Kee Y, Zhou D, Wang Y, Spincemaille P. Preconditioned total field inversion (TFI) method for quantitative susceptibility mapping. *Magn Reson Med*. 2017;78(1):303–15.
- Liu Z, Spincemaille P, Yao Y, Zhang Y, Wang Y. MED+0: morphology enabled dipole inversion with automatic uniform cerebrospinal fluid zero reference for quantitative susceptibility mapping. *Magn Reson Med*. 2018; 79(5):2795–803.
- Liu T, Wisnieff C, Lou M, Chen W, Spincemaille P, Wang Y. Nonlinear formulation of the magnetic field to source relationship for robust quantitative susceptibility mapping. *Magn Reson Med*. 2013;69(2):467–76.

39. Brunori M. Hemoglobin: structure, function, evolution, and pathology. *Trends Biochem Sci.* 1984;9(5):176.
40. Billett H. Hemoglobin and hematocrit. In: rd, Walker HK, hall WD, Hurst JW, editors. *Clinical methods: the history, physical, and laboratory examinations.* Boston: Butterworth Publishers, a division of Reed Publishing; 1990.
41. Ludbrook J. Linear regression analysis for comparing two measurers or methods of measurement: but which regression? *Clin Exp Pharmacol Physiol.* 2010;37(7):692–9.
42. Golay X, Silvennoinen MJ, Zhou J, Clingman CS, Kauppinen RA, Pekar JJ, van Zijl PCM. Measurement of tissue oxygen extraction ratios from venous blood T2: increased precision and validation of principle. *Magn Reson Med.* 2001; 46(2):282–91.
43. Fernández-Seara MA, Techawiboonwong A, Detre JA, Wehrli FW. MR susceptometry for measuring global brain oxygen extraction. *Magn Reson Med.* 2006;55(5):967–73.
44. Fan AP, Benner T, Bolar DS, Rosen BR, Adalsteinsson E. Phase-based regional oxygen metabolism (PROM) using MRI. *Magn Reson Med.* 2012;67(3):669–78.
45. Haacke EM, Lai S, Reichenbach JR, Kuppusamy K, Hoogenraad FGC, Takeichi H, Lin W. In vivo measurement of blood oxygen saturation using magnetic resonance imaging: a direct validation of the blood oxygen level-dependent concept in functional brain imaging. *Hum Brain Mapp.* 1997;5(5):341–6.
46. Weisskoff RM, Kiihne S. MRI susceptometry: image-based measurement of absolute susceptibility of MR contrast agents and human blood. *Magn Reson Med.* 1992;24(2):375–83.
47. Jain V, Abdulmalik O, Probert KJ, Wehrli FW. Investigating the magnetic susceptibility properties of fresh human blood for noninvasive oxygen saturation quantification. *Magn Reson Med.* 2012;68(3):863–7.
48. Haacke EM, Tang J, Neelavalli J, Cheng YCN. Susceptibility mapping as a means to visualize veins and quantify oxygen saturation. *J Magn Reson Imaging.* 2010;32(3):663–76.
49. Cho J, Kee Y, Spincemaille P, Nguyen TD, Zhang J, Gupta A, Zhang S, Wang Y. Cerebral metabolic rate of oxygen (CMRO2) mapping by combining quantitative susceptibility mapping (QSM) and quantitative blood oxygenation level-dependent imaging (qBOLD). *Magn Reson Med.* 2018; 80(4):1595–604.
50. Zhang J, Cho J, Zhou D, Nguyen TD, Spincemaille P, Gupta A, Wang Y. Quantitative susceptibility mapping-based cerebral metabolic rate of oxygen mapping with minimum local variance. *Magn Reson Med.* 2018; 79(1):172–9.
51. Barratt-Boyes BG, Wood EH. The oxygen saturation of blood in the venae cavae, right-heart chambers, and pulmonary vessels of healthy subjects. *J Lab Clin Med.* 1957;50(1):93–106.
52. Wagner A, Mahrholdt H, Thomson L, Hager S, Meinhardt G, Rehwald W, Parker M, Shah D, Sechtem U, Kim RJ, Judd RM. Effects of time, dose, and inversion time for acute myocardial infarct size measurements based on magnetic resonance imaging-delayed contrast enhancement. *J Am Coll Cardiol.* 2006;47(10):2027–33.
53. Aime S, Caravan P. Biodistribution of gadolinium-based contrast agents, including gadolinium deposition. *J Magn Reson Imaging.* 2009;30(6):1259–67.
54. Deshmane A, Gulani V, Griswold MA, Seiberlich N. Parallel MR imaging. *J Magn Reson Imaging.* 2012;36(1):55–72.
55. Lustig M, Donoho D, Pauly JM. Sparse MRI: The application of compressed sensing for rapid MR imaging. *Magn Reson Med.* 2007;58(6):1182–95.
56. Sun H, Wilman AH. Quantitative susceptibility mapping using single-shot echo-planar imaging. *Magn Reson Med.* 2015;73(5):1932–8.
57. Quick HH, Ladd ME, Hoevel M, Bosk S, Debatin JF, Laub G, Schroeder T. Real-time MRI of joint movement with trueFISP. *J Magn Reson Imaging.* 2002;15(6):710–5.
58. Larson AC, White RD, Laub G, McVeigh ER, Li D, Simonetti OP. Self-gated cardiac cine MRI. *Magn Reson Med.* 2004;51(1):93–102.
59. Xu B, Spincemaille P, Chen G, Agrawal M, Nguyen TD, Prince MR, Wang Y. Fast 3D contrast enhanced MRI of the liver using temporal resolution acceleration with constrained evolution reconstruction. *Magn Reson Med.* 2013;69(2):370–81.
60. Dewey M, Teige F, Schnapf D, et al. Noninvasive detection of coronary artery stenoses with multislice computed tomography or magnetic resonance imaging. *Ann Intern Med.* 2006;145(6):407–15.
61. Nguyen TD, Spincemaille P, Prince MR, Wang Y. Cardiac fat navigator-gated steady-state free precession 3D magnetic resonance angiography of coronary arteries. *Magn Reson Med.* 2006;56(1):210–5.
62. Nguyen TD, Nuval A, Mulukutla S, Wang Y. Direct monitoring of coronary artery motion with cardiac fat navigator echoes. *Magn Reson Med.* 2003; 50(2):235–41.
63. Nguyen TD, Spincemaille P, Cham MD, Weinsaft JW, Prince MR, Wang Y. Free-breathing 3D steady-state free precession coronary magnetic resonance angiography: comparison of diaphragm and cardiac fat navigators. *Journal of magnetic resonance imaging : JMIR.* 2008;28(2):509–14.

Publisher's Note

Springer Nature remains neutral with regard to jurisdictional claims in published maps and institutional affiliations.

Ready to submit your research? Choose BMC and benefit from:

- fast, convenient online submission
- thorough peer review by experienced researchers in your field
- rapid publication on acceptance
- support for research data, including large and complex data types
- gold Open Access which fosters wider collaboration and increased citations
- maximum visibility for your research: over 100M website views per year

At BMC, research is always in progress.

Learn more biomedcentral.com/submissions

